4 Frequency- and time-dependent effects

The dynamical properties of QPC systems have motivated a significant number of theoretical and experimental investigations not least because of potential device applications. In the following, the appropriate theory and the accompanying experimental evidence are presented.

4.1 Overview of the theory

Although the transport properties of QPCs are well understood in the low-frequency limit very few studies have been performed in the time domain where the electronic motion through the QPC itself will most clearly reflect the wave nature of the transmitted electrons. One theoretical approach lies in the numerical solution of the time-dependent Schrödinger equation [89C, 92E]. Using a finite difference method the time evolution of a Gaussian wavepacket prepared at the entrance to a QPC can be followed (see Figs. 80, 81 and 82). This method is particularly suitable to study the effects of diffraction within the QPC. The transmitted wave shows clear indications of diffracted

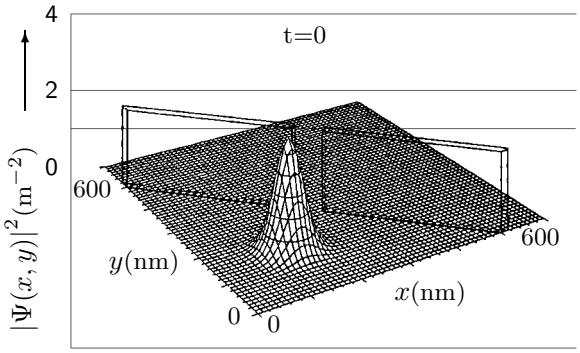

Fig. 80: The time evolution of a Gaussian wavepacket $|\psi(x,y,t)|^2$ is illustrated for the case of a QPC barrier of width 50 nm and length 10 nm (shown only in Fig. 80), for $t = 0$ [92E].

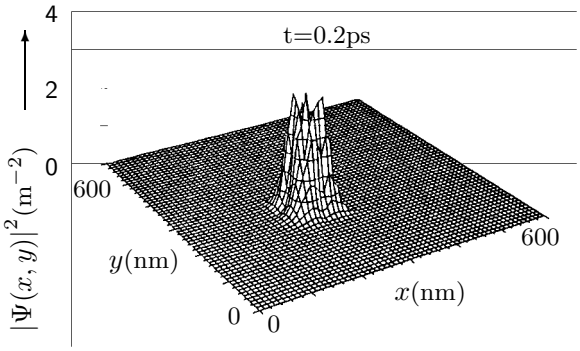

Fig. 81: As in Fig. 80 for $t = 0.2$ ps [92E].

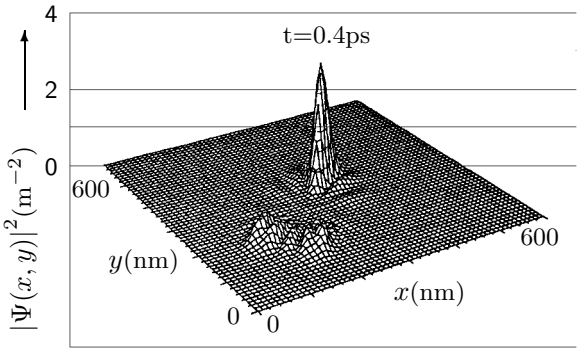

Fig. 82: As in Fig. 80 for $t = 0.4$ ps [92E].

side-peaks which originate from the middle of the QPC entrance. The lateral wave number of the diffracted peaks scales linearly with the diffraction peak index, which reflects the quantization of transverse momentum. Furthermore, it is independent of the channel length, which serves only to determine the number of peaks transmitted, i.e. only those not lying within the geometrical shadow of the exit aperture. Furthermore, the energy of the incident beam together with the channel width determine the direction of propogation of the diffracted beams which emerge from the QPC with a finite time delay. Comparable results have been obtained earlier [89C] which confirm the qualitative features discussed above.

4.1.1 Frequency-dependent effects in quantized transport

One of the first treatments of the high-frequency behaviour of QPCs [92L1] shows that the transport properties can be divided into two distinct regimes. For frequencies $\omega < \tau_L^{-1}$, where τ_L is the transit time along the QPC, the static limit is recovered and it is expected that the device properties are independent of the detailed shape of the potential as expected for an adiabatic system. For frequencies $\omega > \tau_L^{-1}$ the transport properties are determined by a set of coupled equations for the current density, microscopic potential and charge density whose exact solution depends upon the details of the QPC device.

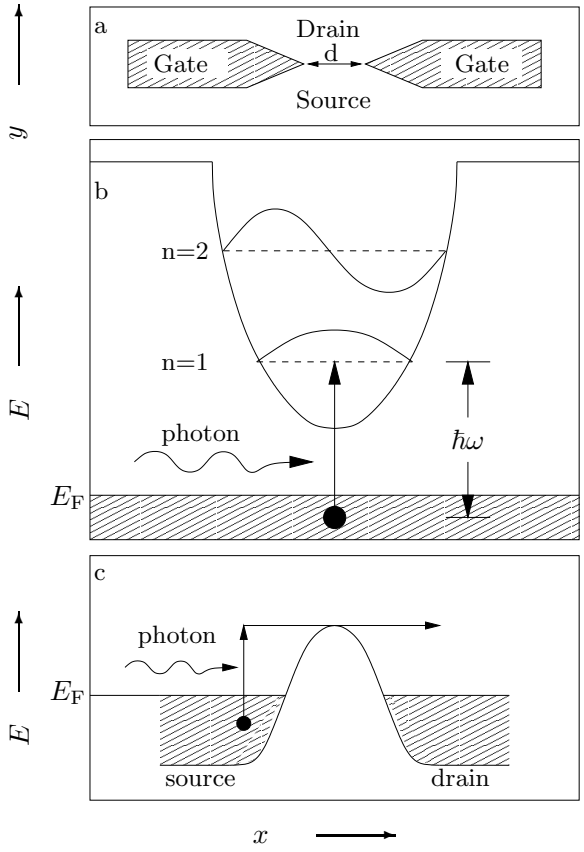

Fig. 83: Schematics of a) the QPC gate electrodes, b) the subband energy scheme relative to the Fermi energy of the reservoirs, and c) the potential profile along the direction of current flow between source and drain [93H2].

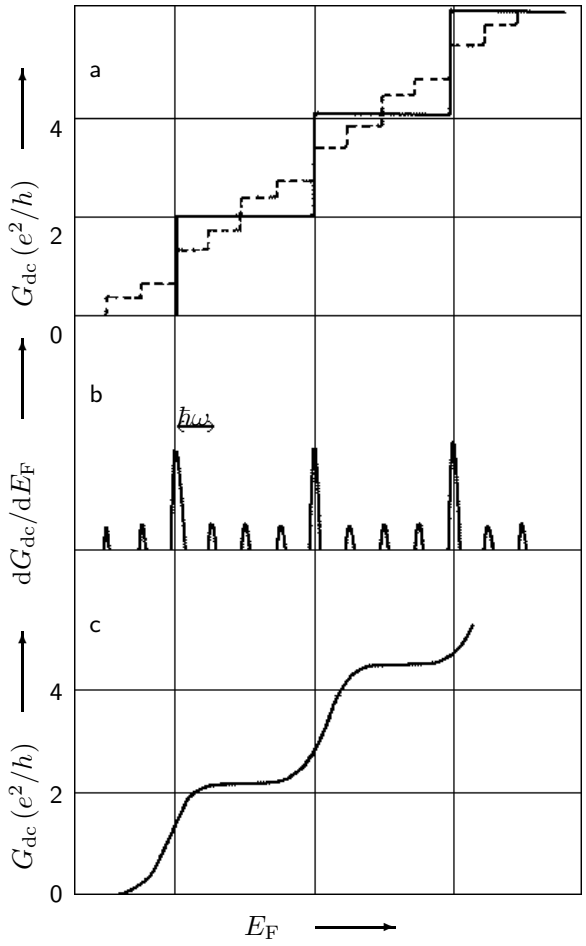

Fig. 84: a) The steplike conductance of a typical QPC device is shown as a function of the Fermi energy (or equivalently gate-voltage). The dotted line indicates the photoinduced response. Also shown are b) the differential photoinduced response with typical sidebands and c) the thermal broadening of the original conductance characteristic [93F2].

4.1.2 Photon-assisted tunneling

In analogy with the photon-assisted transport of quasiparticles in superconducting tunnel junctions it has been proposed that in ballistic QPCs the electronic transport will be similarly modified in the presence of coherent far-infrared radiation [93H2, 93F2]. In pinch-off, when the QPC channel width is sufficiently narrow that the one-dimensional subband energies lie above the Fermi energy,

an enhanced tunneling current can be expected when photon absorption provides an electron in the source reservoir with sufficient energy to pass through the QPC. This situation is illustrated in Fig. 83.

According to the model of Tien and Gordon [63T] the current through a tunnel junction in the presence of a high-frequency field is given by

$$I(V_{\mathrm{sd}}, \alpha) = \sum_{n=0}^{\infty} I_0(V_{\mathrm{sd}} \pm n\hbar\omega) J_n^2(\alpha) \tag{63}$$

where $I_0(V)$ is derived from the DC characteristics and $\alpha = eV/\hbar\omega$ is a parameter which is determined by the amplitude of the applied high-frequency field $V\cos\omega t$. From the above formulation it can be seen that the effect of the high-frequency field is to produce additional echoes of the original DC characteristics which are shifted in energy and weighted by the square of the appropriate Bessel function. For a QPC device in the tunneling regime when $\hbar\omega$ is sufficiently large to promote electrons from the Fermi sea into the first subband the photon induced current is expected to scale with $J_1^2(\alpha)$ and will therefore be proportional to the intensity of the far-infrared radiation [93H2].

A more detailed analysis of photon-assisted tunneling in QPCs [93F2] based upon an adiabatic treatment of the slowly varying confinement potential arising from the gate-electrodes has shown that the problem can be treated within the Tien and Gordon framework above, regardless of the polarization of the high-frequency field. In the linear response limit the gate voltage characteristics are expected to be modified as illustrated in Fig. 84 and ministeps in the conductance are predicted.

As discussed previously (Chapter 3.10), in the nonlinear regime additional plateaux in the conductance are expected. Such steps in the conductance with increasing V_{sd} will also be reflected in the photoresponse and comparable ministeps should be observed. In a realistic device free carrier absorption in the surrounding 2DEG will inevitably accompany the photoresponse. The associated heating of the electron gas will mask the photon-assisted signal and an efficient coupling of the far-infrared radiation to the QPC [93H2, 93F2] is therefore essential.

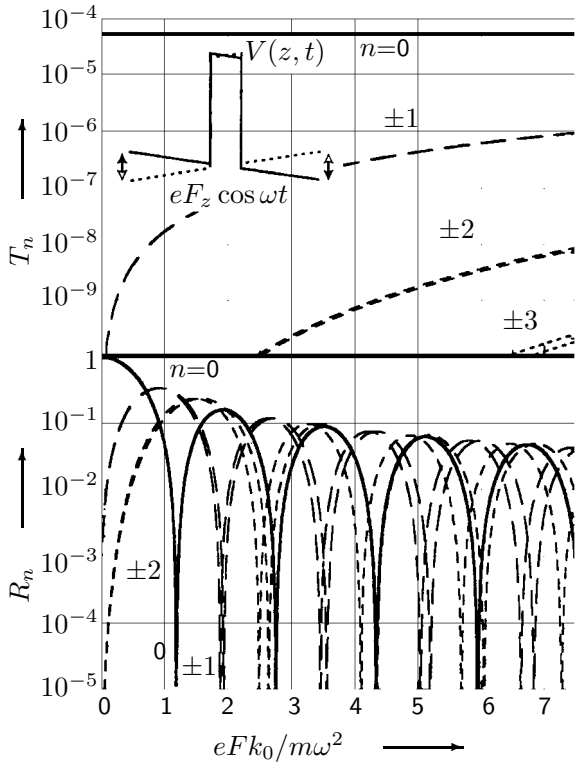

Fig. 85: The transmission and reflection probabilities for a single barrier driven by the AC field $eFz\cos\omega t$ are shown as a function of the scaling parameter $eFk_0/m\omega^2$ [97W].

In the model of Tien and Gordon the potential is assumed to drop completely over the tunnel barrier, and the AC potential serves only to modulate the otherwise spatially uniform potential

of one reservoir. Although this assumption is valid in the superconducting tunnel junctions it is questionable whether it is applicable for ballistic QPCs [97W]. An alternative description of photon-assisted tunneling based upon a linear voltage drop $V_{\mathrm{AC}} = eFz\cos\omega t$ over the active device region (i.e. with constant electric field) yields a very different picture for the transmission and reflection probabilities (see Fig. 85). The transmission occurs predominantly in the centre band $n = 0$ with only weak contributions from the photon-assisted sidebands. The reflection probabilities however, are significantly influenced via the interaction with the AC field and show pronounced oscillatory behaviour as a function of the scaling parameter $eFk_0/m\omega^2$ where k_0 is the incident wavevector. Interestingly, this scaling parameter manifests an ω^{-2} dependence rather than the ω^{-1} dependence expected from the simple Tien and Gordon model, and has been confirmed in other theoretical treatments [99C].

4.1.3 Infrared absorption

The lateral dimensions of QPC devices are such that the intersubband energies are typically of the order of a few meV and comparable with far-infrared photon energies. An asymmetric QPC geometry with variable width has been suggested as a far-infrared detector [93F1] and the associated subband structure is illustrated in Fig. 86. With the device operating in the tunneling regime the

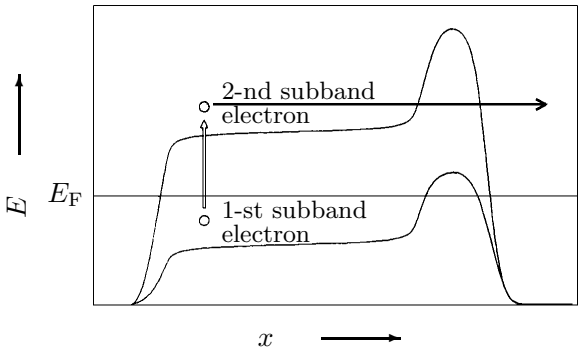

Fig. 86: The subband diagram of the proposed far-infrared QPC detector is shown as a function of the longitudinal channel coordinate [93F1].

dark current through the QPC is negligible. Intersubband absorption within the QPC can give rise to a finite photocurrent if the coupling between first and second subbands is efficient within the narrowest region of the QPC. This transition can be enhanced by an asymmetric variation of the channel width designed to provide an optimal overlap. The above model has been considered theoretically based upon a mode-matching technique within the non-uniform waveguide defined by the QPC. Although the conversion efficiency, defined in terms of a transfer coefficient, was found to be quite weak, it was suggested that the asymmetric QPC geometry could nevertheless operate as a sensitive photovoltaic device with a maximal responsivity of up to 20 mA/W at a photon energy of 5 meV. Furthermore since this effect relies upon the intersubband spacing within the QPC device it is expected to operate as a selective, tunable detector.

The asymmetry of the above suggestion results from the lack of mirror symmetry along the transport axis of the QPC device. Similarly, a lack of mirror symmetry about the gate-electrode axis (i.e. perpendicular to the current flow) can also result in a photovoltaic response [91H1]. For a time-dependent modulation of the gate electrodes in such a geometry intersubband transitions at resonant points can give rise to a net electron-current flow towards the drain when the resonant point is located on the source side of the QPC. Furthermore it is expected that an integer number of electrons will be transmitted per absorbed photon in such a device.

The optical absorption in an adiabatic QPC constriction has been calculated [94G2] by considering the dipole interaction between the electronic states of the QPC and the photon states of a resonator cavity. It has been shown that the absorption is essentially independent of the QPC geometry and that the optical spectra reflect the form of the lateral confining potential. In particular the absorption at the centre of the QPC is expected to dominate the spectra at high

energies thus enabling the contribution from the QPC to be separated from the absorption in the wide contact regions. For hard wall potentials the energy level separation

$$\Delta E = \frac{(2n+1)\pi^2\hbar^2}{2m^* d_{\min}^2} \tag{64}$$

at the centre of the QPC gives rise to a series of discrete peaks in the absorption, in contrast with a single peak for parabolic confinement.

The above analysis can be extended to determine the photoconductance in a QPC device exposed to high-frequency radiation [95G]. The polarization of the electromagnetic field is transverse to the direction of current flow as required for good intersubband coupling between the modes of the QPC, and the QPC geometry is chosen to be symmetrical so that photovoltaic effects play no role. The absorption of a photon can promote an electron from a conducting subband into a non-conducting subband and acts therefore as an effective backscattering process. As the channel width, or equally the Fermi energy, is varied such backscattering can either enhance or reduce the conductance depending upon whether the initial occupied state is located in the source or drain reservoir. The resulting modified total conductance is shown in Fig. 87 and it is interesting to observe that the amplitude of the photoconductance increases with increasing subband index. The oscillatory photoconductance signal is expected to modify the DC conductance up to a cutoff

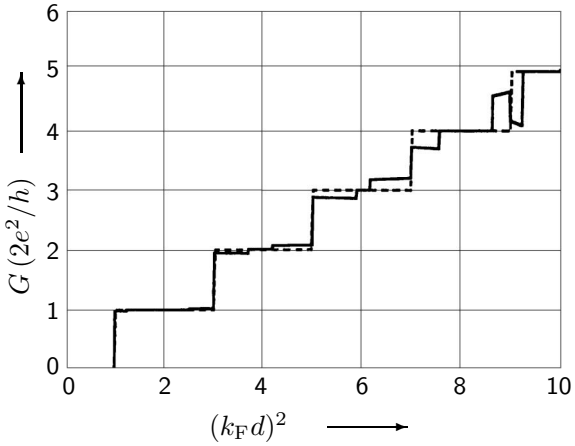

Fig. 87: The conductance of the QPC as a function of the dimensionless parameter $(k_\mathrm{F}d)^2 \propto E_\mathrm{F}$ [95G]. The solid line shows the photoconductance with additional step structure becoming more pronounced for higher subband index.

subband index, whose value is determined by the frequency of the radiation and decreases with increasing frequency.

An exact numerical analysis of the photoconductance through QPCs has confirmed the essential features of the approximate, analytic theory discussed above [96M2]. The oscillatory behaviour of the photoconductance is however expected to be enhanced due to quantum, nonadiabatic corrections, resulting from the use of semiclassical wavefunctions in earlier models. These exact calculations have been extended to include the effects of an impurity located close to the entrance of the QPC device [96M1]. Not suprisingly the resultant asymmetry of this configuration gives rise to a photovoltaic response which can be understood naïvely as an enhanced transmission, or ballistic rectification, arising from scattering off the impurity potential.

The interaction of far infrared radiation with the modes of a ballistic one-dimensional channel has been investigated [97T1] and it has been predicted that resultant mode population will vary along the channel length. The intensity of the radiation controls the period of this spatial modulation and the phenomenon can be compared qualitatively with Rabi oscillations, where, due to the electronic motion, the transitions are spatial rather than temporal. A novel multiple QPC geometry has been proposed which, when driven with appropriate time-dependent electrode voltages, leads to the definition of a moving QPC. This dynamic QPC can be exploited to measure the local mode population along the channel, and oscillations in the current are predicted where the period is proportional to the wavelength of the spatial modulation within the channel. A further

novel prediction for ballistic one-dimensional channels is the blockage of current transport through a ballistic QPC in the presence of far infrared radiation [98T]. The important assumption is that of an almost parabolic confining potential such that the coherent pumping with the infrared field leads to a significant depopulation of the lowest modes within the channel. The photoconductance, as characterized both by the frequency and field strength of the applied far infrared radiation, is expected to yield spectroscopic information about the modes within the channel. Indeed, it is suggested that the sensitivity of such a QPC device to the infrared field is such that this effect could be exploited for frequency demodulation in the THz range.

4.1.4 Surface acoustic wave spectroscopy

The interaction between a ballistic QPC and a surface acoustic wave (SAW) modifies the current-voltage characteristics according to $I = I^{\rm ac} + GV$ where $I^{\rm ac}$ is the acoustoelectric current and $G = G^{\rm dc} + G^{\rm ac}$ is the sum of two terms, the usual DC conductance and an additional acoustoconductance [97T2]. Both the acoustoelectric effect and the acoustoconductance are expected to scale linearly with the SAW intensity. The effect of the SAW is to cause intersubband transitions which can result in a backscattering of the propogating modes similar to the situation for photoconductance [95G]. Such backscattering is expected to be important at the onset of conduction of the transverse subband modes. Furthermore due to the nature of the backscattering interference between two reflected waves will give rise to oscillatory structure in the acoustoconductance.

4.1.5 Noise phenomena

Classically the shot noise due to the uncorrelated motion of electrons in a conductor is given by

$$\langle (\Delta I)^2 \rangle = 2e\Delta\nu I \tag{65}$$

where $\Delta\nu$ is the bandwidth of the measurement. For QPC systems, where a limited number of modes are almost perfectly transmitted, the above result must be modified accordingly [89L2, 90Y2],

$$\langle (\Delta I)^2 \rangle = \frac{2e^2}{h} \Delta\nu |eV| \sum_n T_n (1 - T_n). \tag{66}$$

This formula, which reduces to the classical result in the limit when all modes are weakly transmitted was initially derived for a two-terminal conductance measurement in the absence of scattering between modes, and has subsequently been extended to multiterminal systems in the presence of magnetic fields with an arbitrary scattering matrix [90B3]. In QPC devices the bimodal distribution of T_n ensures that the shot noise is zero when a finite number of modes are perfectly transmitted, and has a nonvanishing component only when $E_n = E_{\rm F}$, i.e. as each mode switches into the conductance and the associated transmission coefficient changes from zero to unity. At $E_n = E_{\rm F}$ the shot noise is maximal and scales with either $(eV)^2/k_{\rm B}T$ or $(eV)^2/\Delta_n$ when $\Delta_n \gg k_{\rm B}T$ or $k_{\rm B}T \gg \Delta_n$ respectively. Here Δ_n is the energy scale over which the mode switches into the conductance and is, in the adiabatic approximation, given by $\Delta_n = n\hbar^2/m\sqrt{2Rd^3}$ as discussed previously (see Section 3.1.1 above). Similarly, the equilibrium noise in a mesoscopic conductor can de determined using the scattering matrix approach and yields

$$\langle I_\alpha^2 \rangle = 4\Delta\nu k_{\rm B}T \frac{e^2}{h} \int {\rm d}E \left(-\frac{{\rm d}f}{{\rm d}E} \right) \sum_{\beta \neq \alpha} T_{\alpha\beta} \tag{67}$$

where $T_{\alpha\beta}$ is the total transmission probability between contacts α and β. For a two-terminal measurement this reduces to the familiar Johnson-Nyquist noise formula $\langle I^2 \rangle = 4\Delta\nu k_{\rm B}TG$ where G is the device conductance, and equivalently for the voltage fluctations between two contacts $\langle (V_\alpha - V_\beta)^2 \rangle = 4\Delta\nu k_{\rm B}TR$ where R is the two-terminal resistance [90B3].

Similar results have been obtained assuming an adiabatic QPC geometry and a symmetric voltage drop along the device channel [92EY]. The resulting analytical expression can be directly related to the DC current-voltage characteristics of the QPC device and reduces to the form discussed above in the low-temperature limit. The factor $T(1-T)$ found in all of these theoretical approaches reflects the mean square deviation of the average level occupancy within the QPC modes, and demonstrates that the low-temperature transport through a QPC is correlated [90B3, 92EY]. The suppression of the shot noise is therefore a direct consequence of the strongly reduced fluctuation of the occupancy of the fermionic states within the constriction.

A more extensive theoretical treatment [92B2], again based upon the scattering matrix approach, has emphasized the fundamental connection between the statistical properties of a system of identical non-interacting particles, as expressed in the current-current correlations, and the low-temperature transport properties of QPC-like mesoscopic geometries. For both fermions and bosons the equilibrium noise between two contacts, as given by the fluctuations in the particle flux, is found to be negative. The shot noise contributions to the fluctuation are, in contrast, negative for fermions and positive for bosons. Such current-current correlations are, of course, the electronic analog of the second-order coherence as found in optical experiments [56HB] and therefore form the theoretical basis for the investigation of the statistical phenomenon of "fermionic antibunching" and related effects as discussed in Section 3.9 above.

Another source of low-frequency noise in ballistic QPCs results from time-dependent scattering potentials acting upon the injected electrons. Possible mechanisms invoked to explain such potential fluctuations include electron hopping between neighbouring impurity centres as well as the vibrational motion of atoms in so-called two-level tunneling systems. Such dynamic defects produce a slowly varying potential which scatters the conduction electrons, and have been theoretically considered [95H1] as an explanation for the observed time dependent conductance in QPC devices. In an adiabatic model the influence of the time dependent potentials is incorporated by including a spatially homogeneous potential variation $\delta u(t)$ of the lateral confining energies, which reflects the influence of an ensemble of elementary "fluctuators" of varying strength and activation energy. Numerical simulations based upon this model show that the noise level is low in the middle of the plateaux, where the dominant noise contribution comes from the weak fluctuators, whereas between conducting steps the noise is determined by a small number of strong fluctuators located close to the channel. The frequency dependence of the noise spectrum is predicted to have the form: $S(\omega) \propto 1/\omega^{\alpha}$ above a critical frequency ω_c which can be related to the transition rate between states of the fluctuators. The exponent α is expected to be less than 1 and to be weakly enhanced on the conductance plateaux.

While the above model can be intuitively understood as arising from the time dependence of the effective channel geometry, and hence the channel transmission within the adiabatic approximation, an alternative, complementary picture based upon a coherent mode mixing has been suggested [95H2]. Coherent mode-mixing has been previously invoked (see Section 3.1.10) as a source of nonlinear behaviour in QPCs [94Z] to explain transport phenomena in the limit $eV_{sd} \ll \Delta E$. Here, one of the two scattering centres responsible for the intermode mixing is presumed to have the time-dependent behaviour characteristic of an elementary fluctuator in contact with a thermal bath. In the context of the coherent mixing model this leads to discrete time-dependent phase shifts and hence to the occurence of random telegraph noise. The derived noise spectrum $S(\omega)$ is the product of three factors: $[\cosh(\Delta/2k_BT)]^{-2}$, which reflects the interaction of the elementary fluctuator with the thermal bath, $L(\omega) = \Gamma/(\Gamma^2 + \omega^2)$, a Lorentzian of width characteristic of the activation energy, and a term proportional to the mean square amplitude of the current fluctuations. The dominant contribution to the noise is found in general to come from mode mixing between the lowest two channel modes. Furthermore the period of the noise oscillations as a function of external parameters (e.g. V_g) is expected to be half the period of the current oscillations predicted by the model.

The influence of intermode scattering has also been considered within the context of the coupling of a QPC to an electrodynamic environment [91H2]. Fluctuations of both the gate voltage

and source-drain voltage can lead to inter- and intrachannel scattering; for adiabatic constrictions intrachannel scattering is predicted to be more important than interchannel scattering and the source-drain voltage fluctuations contribute more strongly than those of the gate electrodes. Furthermore the low-frequency response is characterized by a universal frequency-dependent conductance regardless of the exact potential distribution within the QPC.

Both the quantum statistical shot and equilibrium noise as well as the flicker noise discussed above are low-frequency noise sources. In the high-frequency limit deviations from the white noise spectrum expected for shot noise have been observed in diffusive conductors [97S1], and have motivated theoretical investigations of this limit [98P]. At high frequencies fluctuations of the current within a QPC device couple capacitatively to the surrounding environment, for example to the gate electrode used to define the QPC, and induce current fluctuations in the environment which depend upon the charge dynamics of the QPC itself. Such fluctuations can be characterized by a dynamical resistance related to the density of states matrix. In contrast with the low-frequency shot and equilibrium noise, which are entirely determined by the transmission (i.e. scattering matrix of the system), the induced high-frequency fluctuations manifest the dynamical properties of the system as expressed in the energy derivative of the scattering matrix. Detailed investigations [98P] have shown that this dynamic resistance reflects the quantized nature of the transverse states within the QPC, as seen in the 1D density of states.

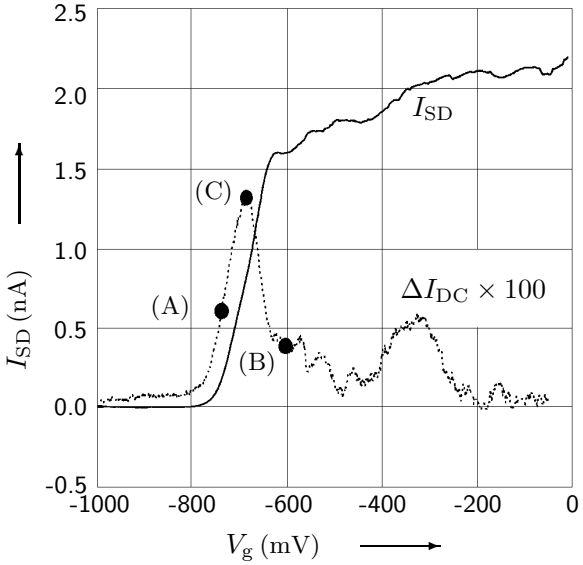

Fig. 88: The DC current (solid curve) for an applied bias of 100 μV is shown as a function of QPC bias voltage. The dotted trace shows the induced current [94K2].

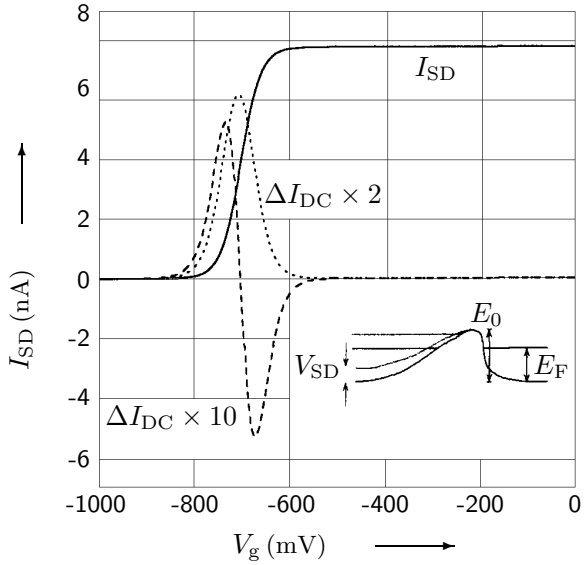

Fig. 89: The calculated DC current (solid curve) and simulations of the induced current with the AC signal applied to the source-drain bias (dotted curve), or as a modulation of the gate induced barrier height [94K2].

4.2 Frequency-dependent effects in quantized transport

The high-frequency response of QPC devices operating in the nonlinear regime have been investigated [94G1, 97H2] because of their possible device applications as discussed more fully in Section 5.2. These experiments were performed at frequencies up to approximately 10 GHz, which is significantly lower than the critical frequency discussed above [92L1], and can therefore be well described with the observed DC transport characteristics. At somewhat higher frequencies ($f \leq 200$ GHz) the dynamic response of a QPC, defined in a thin channel with a single gate electrode, has been measured [94K2] using a time-domain interferometer, which permits the frequency

response to be characterized. The observation of an induced DC current confirms previous reports of the FIR response of ballistic QPCs and is illustrated in Figs. 88 and 89.

The observation of a unipolar induced current signal suggests that the effective high-frequency radiation couples most effectively to the two-dimensional contact regions and modulates the source-drain bias accordingly. The observed frequency response showed an essentially flat response with resonant features attributed to the frequency dependent coupling to the device through the bond wires.

4.3 Photon-assisted tunneling

The original suggestion that photon-assisted tunneling could be observed in QPC devices [93H2] correctly stressed the importance of coupling the far infrared radiation to the active region of the device and equally of minimizing the inevitable bolometric effects in the surrounding reservoirs. Indeed, the integration of the gate eletrodes into the design of an efficient broadband antenna with a polarization perpendicular to the device current provides a simultaneous solution to both these problems. Nevertheless, the observation of clear frequency dependent signals correlated with the energy of the individual photons in the radiation field remains elusive: the majority of QPC experiments show a predominantly bolometric response [96H] as discussed in Section 4.4 below. The absence of photon-assisted tunneling has been attributed to the exponential dependence of the photon-excited transition probability upon the localization of the high-frequency field. An appreciable transition probability requires a significant spatial confinement of either the electronic states or the high-frequency field on a length scale $1/\Delta k$ given by the momentum change induced by the photon absorption. In QPC devices, with electronic states which extend far into the surrounding 2D reservoirs, such localization of the high-frequency field has not been attained despite the use of impedance matched, broadband antenna configurations and nanostructured geometries. These observations are in marked contrast to those of quantum dot devices where the confinement of the electronic states yields the necessary momentum transfer for the photon assisted processes.

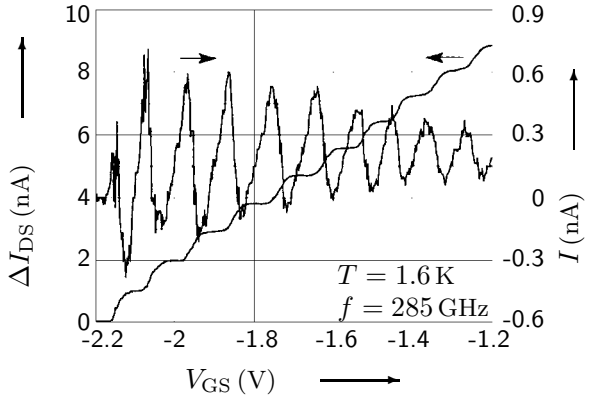

Fig. 90: The photon-induced current is shown as a function of the applied gate voltage, as is the conductance in the absence of far infrared radiation [93W].

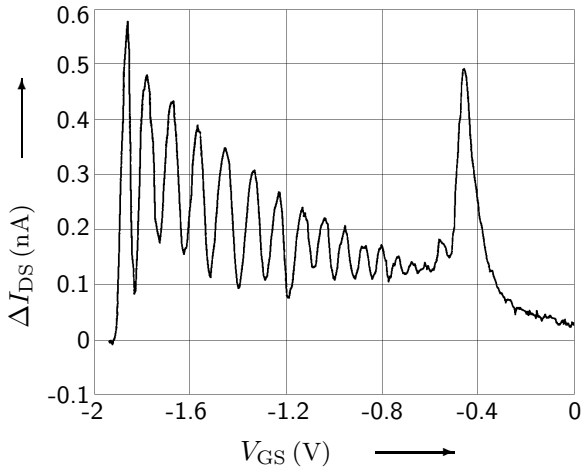

Fig. 91: The thermally induced source-drain current, i.e. the difference between the conductances measured at 3.7 and 1.6 K, is plotted as a function of the applied gate bias [93W].

4.4 Infrared absorption

The first reported broadband investigation of the far infrared photoresponse of ballistic QPCs [93W] was in fact designed to investigate photon-assisted transport in such devices. The far infrared radiation was focussed using a log-periodic antenna integrated into the gate electrodes and yielded an electric field orthogonal to the source-drain current. Although such a field orientation is different from that assumed in the Tien and Gordon model, a similar photon assisted signal has been theoretically predicted [93F2]. Nevertheless the observed photoresponse (as illustrated in Fig. 90) cannot be explained within the framwork of photon assisted tunneling. The observed oscillations, which are predominantly positive below the threshold of the conductance steps and negative above, are more suggestive of a bolometric response of the QPC device. A qualitative confirmation of this hypothesis is presented in the data of Fig. 91, where the temperature variation of the QPC device conductance is shown.

Similar oscillatory behaviour under the influence of far infrared radiation has been observed [94J] even in the absence of an applied bias current (see Fig. 92). Electron heating has been discounted as a possible mechanism for this signal both from a quantitative analysis as well as from the zero bias observation of a rectified signal. It was suggested that classical rectification is the most plausible mechanism for the origin of this signal and the observed data were compared with the second derivative of the current-voltage characteristics as shown in Fig. 93. The frequency

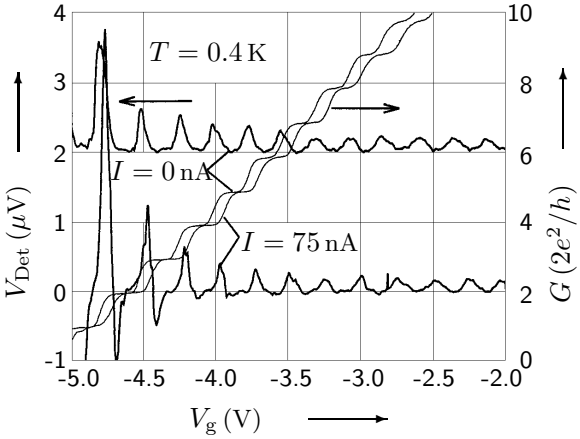

Fig. 92: The simultaneously measured photoresponse and conductance of a ballistic QPC exposed to far infrared radiation ($f = 525\,\mathrm{GHz}$) for two different bias conditions [94J].

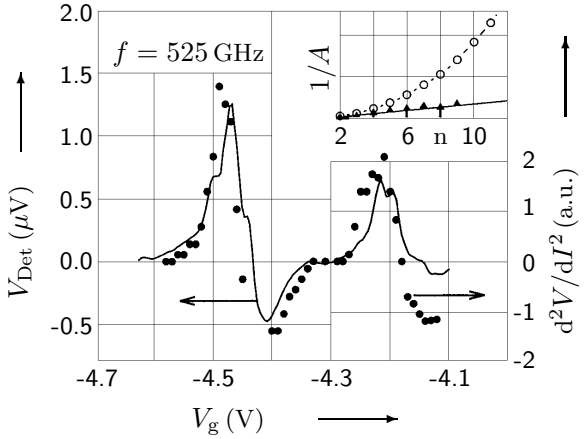

Fig. 93: The photoresponse for an applied bias current of 75 nA and the second derivative of the DC current-voltage characteristics are shown as a function of the applied gate voltage [94J]. The inset shows the inverse amplitude of the detector signal as a function of the subband index.

dependence of this rectification mechanism has been investigated at discrete frequencies up to roughly 2.5 THz [95A]. The measured photocurrent was compared with the second derivative $\mathrm{d}^2I/\mathrm{d}V_{\mathrm{sd}}^2 = \mathrm{d}G/\mathrm{d}V_{\mathrm{sd}}$ of the current-voltage characteristics, and for frequencies below roughly 1 THz excellent quantitative agreement is found. The fit parameter β varied with polarization and frequency with typical values of the order of $\beta = 0.01$. Beyond 2 THz good qualitative agreement is found with the rectification model, however no single value of β yields a good quantitative fit, leading to the suggestion that at sufficiently high frequencies $f_{\mathrm{c}} \geq 1/\tau_{\mathrm{t}}$, where τ_{t} is the transit time through the QPC, additional mechanisms are responsible for the observed photocurrent.

The observation of a zero bias photoresponse can also result from an antisymmetric coupling between the far infrared radiation field and the device geometry [95W]. The resulting radiation-induced thermopower has been systematically investigated (see Fig. 94), and it has been shown that both the polarity and the magnitude of the induced photocurrent can be tuned by shifting

the 285 GHz far infrared beam even when a symmetric antenna geometry is used. The induced

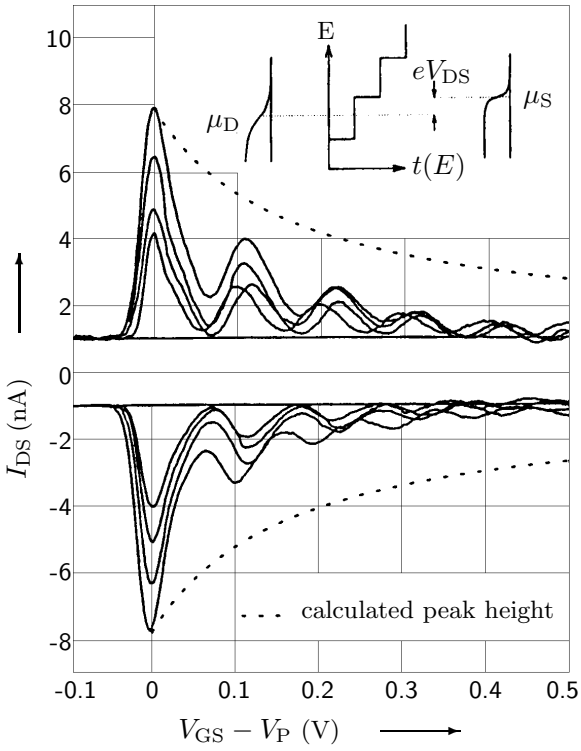

Fig. 94: The photon-induced source-drain current is plotted as a function of gate voltage for a systematic variation of the far infrared beam position without applied source-drain bias [95W]. The dotted line indicates the maximum peak height calculated using a simple analytical model which assumes differential heating in the reservoirs.

photocurrent has been simulated using a simple analytical model and it is expected that $I_{sd} \approx \Delta T_{sd}/n$ should scale with the induced temperature difference between the reservoirs and with the inverse of the number of occupied subbands. With one occupied subband a temperature difference $\Delta T_{sd} = 2.3\,K$ (for a fixed, arbitrary radiation power) has been determined, and the more rapid decay of the photocurrent, attributed to an increased thermal conductance as the subband occupancy increases, observed.

4.5 Surface acoustic wave spectroscopy

The influence of surface acoustic waves (SAW) upon the conductance of ballistic channels is of particular interest due to its potential application as a current standard (see Section 5.2). Initial experimental investigations of such properties [96S1, 96S2] were performed with a SAW wavelength of roughly $1-3\,\mu m$ and ballistic channels of comparable length of $500-700\,nm$.

The acoustoelectric signal observed is clearly correlated with the device conductance (see Fig. 95) and shows oscillatory structure where the maxima of the oscillations coincide with the transitions between conductance plateaux. This effect is an agreement with the theory [97T2] discussed in Section 4.1.4 above, and reflects the matching of the electron velocity with that of the sound wave as the laterally quantized modes switch into the conductance. At high power levels structure in the acoustoelectric current is found beyond pinch-off (see Fig. 96) which corresponds to the transfer of an integer number of electrons per period of the SAW. The first acoustoelectric current plateau shows a well quantized current with a single electron being transferred with each sound wave period. By contrast the second plateau is susceptible to changes in the system parameters and shows a pronounced power dependence.

4.6 Noise phenomena

The first measurements of the noise properties of ballistic QPCs were performed in the low-frequency range, between 100 Hz and 100 kHz [90L]. The noise spectrum was found to contain

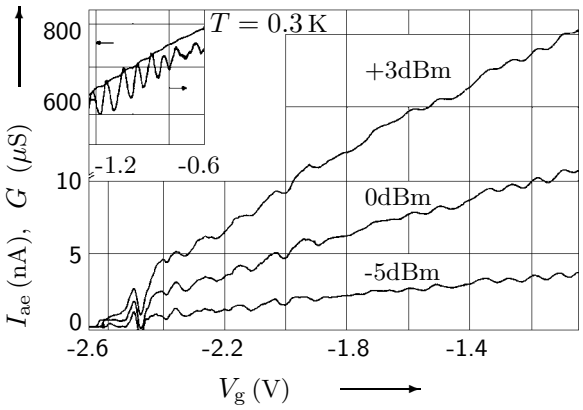

Fig. 95: The acoustoelectric current is plotted as a function of the applied gate voltage for various SAW power levels. The inset shows the correlation between the conductance plateaux and the minima in the acoustoelectric current [96S2].

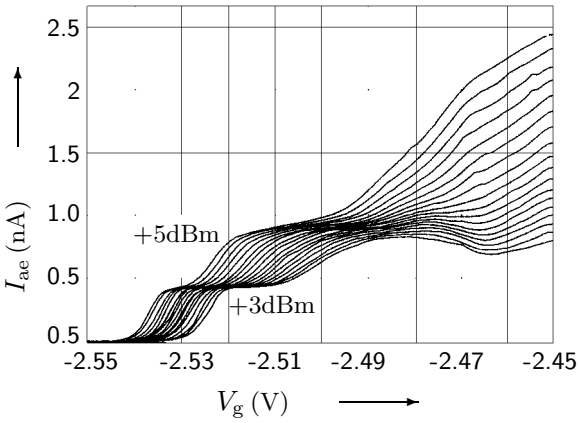

Fig. 96: The acoustoelectric current in the region beyond pinch-off for various SAW power levels ($f_{rf} = 2728.4$ MHz) [96S2].

two components: a $1/f$ component (I^β/f^α with $\beta = 2$ and $\alpha = 0.9$) which manifested oscillatory behaviour with minima at gate voltages corresponding to the conductance plateaux (see Fig. 97), and a white noise component which increases with the source-drain current but is significantly suppressed when compared with the full theoretical shot noise result (see Fig. 98). The $1/f$ noise is attributed to the addition of a monotonically increasing component unrelated to the resistance quantization and a component which is clearly correlated with the 1D subband structure of the QPC, although no specific mechanism is envisaged. The increase of the shot noise is believed to arise from intersubband mixing and from an imperfect adiabatic transmission through the QPC. Another early experimental observation [90T2] of the noise in QPCs attributed the observed suppression to a modulation of the scattering resulting from a single impurity within the constriction of the QPC.

Subsequent investigations [91D, 91L2, 92L2, 94L2] have confirmed and extended the above description of the noise properties, and suggest that the origin of the noise in QPC devices is to be found in the trapping and detrapping of electronic states in the channel vicinity. Significant variations of the noise spectral density were observed in different QPCs and reflect the fundamental mesoscopic character of such devices. In particular one QPC device showed a Lorentzian spectral density and a strikingly different temperature dependence. Nevertheless, the quantum size effect reported previously is confirmed and its origin associated with the sensitivity of the ballistic transmission whenever a mode switches into the conductance. The direct observation of discrete resistance switching in the time domain, as illustrated in Fig. 99, provides supporting evidence for this interpretation; such "random telegraph signals" (RTS) can explain quantitatively the observed Lorentzian noise spectrum and the temperature dependence can be understood as thermally activated behaviour. In the presence of a perpendicular magnetic field the transition from local to global adiabaticity of the transport through the QPC leads to a strong suppression of the noise on the conductance plateaux. This effect is illustrated in Fig. 100 where the observation of additional weakly suppressed minima results from the lifting of the spin degeneracy. The strong suppression of the minima shows a noise level typically one order of magnitude smaller than that observed at $B = 0$. Within the context of the above model where a single trapping centre is associated with a Lorentzian noise spectrum, the observed $1/f$ spectral noise is attributed to an ensemble of traps within the QPC vicinity. The broad range of time constants for the trapping and detrapping processes, required to produce a $1/f$ spectrum, necessitates a flat distribution of activation energies, which would be reflected in the temperature dependence of the noise spectrum.

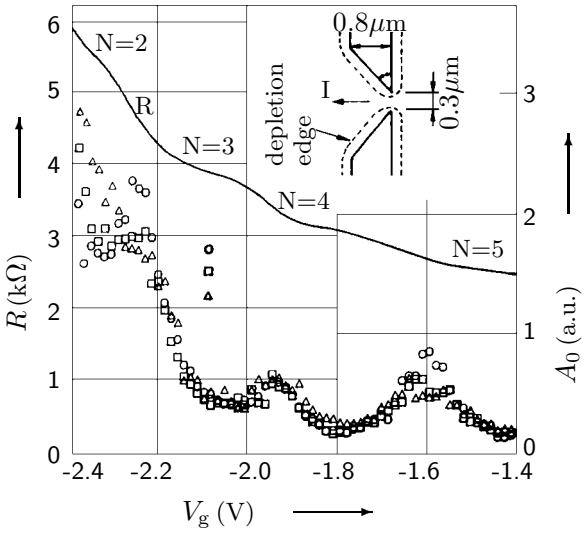

Fig. 97: Both the channel resistance and the $1/f$ noise of a ballistic QPC are plotted as a function of the applied gate bias [90L]. The inset shows the QPC geometry, and the symbols ∘, □, and △ correspond to 0.4 μA, 0.5 μA, and 0.6 μA, respectively.

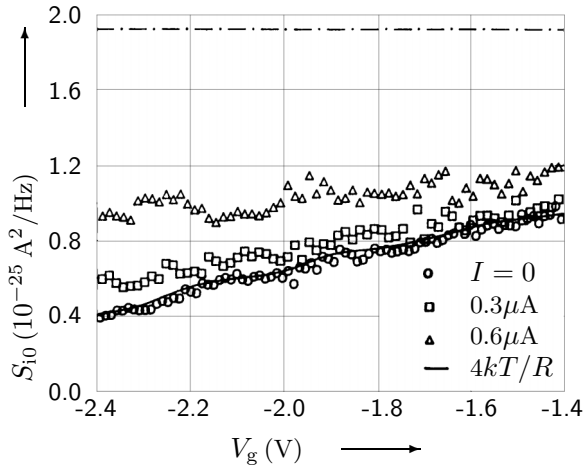

Fig. 98: The white noise spectrum of a ballistic QPC is plotted as a function of the applied gate bias. The full line shows the Johnson noise result $4k_BT/R$ while the dashed line shows the theoretical full shot noise result [90L].

This predicted feature [94L2] has been extracted from comparisons of the data with simple model calculations.

Systematic studies of the "random telegraph signals" in QPCs show a rich and varied behaviour [91C, 92T4, 92C2, 95S1], whose analysis has contributed to the understanding of defect states in QPC devices. The potential modulation introduced through the occupancy of such defect states is most visible in the transition region between quantized conductance plateaux. In the time domain this leads to the observation of so-called quasicharacteristics [91C] when the bandwidth of the gate-voltage sweep is sufficient to resolve the RTS. A detailed analysis of these quasicharacteristics permits the energy shifts associated with the occupancy of the defect states, as well as their approximate positions with respect to the QPC channel to be determined. Furthermore, interactions between two such defect states have also been resolved as illustrated in Fig. 101. The dynamic behaviour of the labelled state B_0/B_-, as defined in terms of its individual occupancy, is clearly influenced by the occupancy of the A_0/A_- state. An elegant extension of the investigation of interacting traps has been found in QPC systems where the device channel can be shifted laterally through the separate biasing of the split-gate electrodes [95S1] with potentials $V_g + \Delta V_g$ and $V_g - \Delta V_g$. In the two-dimensional plane $(\Delta V_g, V_g)$ the RTS signals are clearly observed as lines of large transconductance. Interestingly, clear evidence for anticrossing between these lines is found, and has been interpreted as the blocking of the trapping states through the occupancy of neighbouring traps.

Time-irreversible switching behaviour has been observed in the conductance quasicharacteristics between pinch-off and the first conductance plateau [92C2]. As illustrated in Fig. 102 transitions from the level A to the level O are never observed although the reverse transition regularly occurs within the level scheme shown. The microscopic origin of this irreversibility is presumed to be related to current flow from a gate electrode to the underlying 2DEG through defect states near the channel. An interesting application of a series combination of two QPCs, which has been used previously to perform spectroscopy on the occupied electronic states between the two QPCs (see Section 3.8 above), is to be found when only one of the two QPCs manifests RTS structure [92T4]. Under such circumstances the noise present in a conductance signal has been exploited to

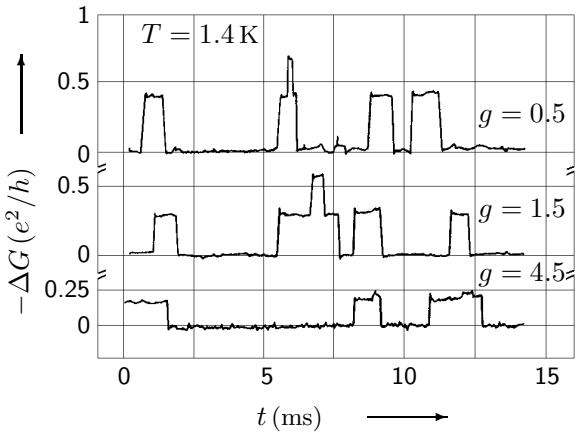

Fig. 99: The conductance of a QPC device with Lorentzian noise spectrum is plotted as a function of time for various values of $g = G/(2e^2/h)$ [91D].

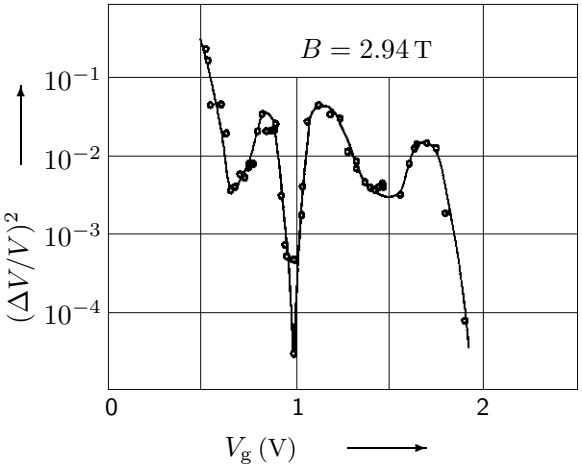

Fig. 100: The voltage noise $(\Delta V/V)^2$ is plotted as a function of the QPC conductance for an applied perpendicular field of $B = 2.94\,\mathrm{T}$ [91L2].

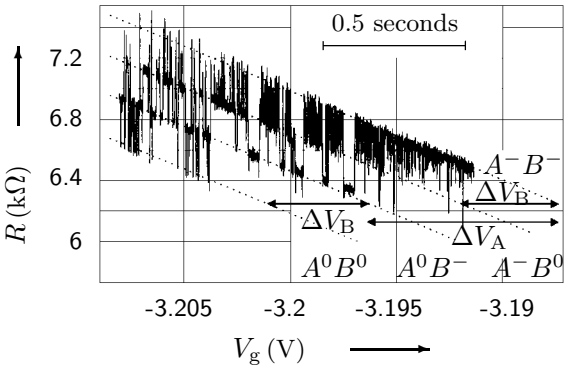

Fig. 101: The channel resistance in the transition region between two quantized plateaux is plotted as a function of the gate voltage during a slow sweep with 2 kHz bandwidth [91C]. The four quasicharacteristics are identified with the four possible occupancy levels of a two defect system.

investigate the electron transport at high magnetic fields. It has been found that the conductance observed is compatible with the complete equilibration of a finite number of current carrying edge states.

RTS have also been observed [96S3, 97S2] in the QPC like structures discussed in Section 3.10 above. Although phenomenologically similar to the experiments discussed above, the RTS observed are found under conditions of high bias corresponding to the strongly nonlinear portion of the current-voltage characteristics considered earlier. As such it is suspected [97S2] that the origin of these RTS is not to be found in the charge traps discussed above, but rather in subband instabilities of the 1D channel. This supposition is supported by measurements of the conductance change between the two well-defined conductance states, and it is found that $\Delta G = \beta(2e^2/h)$ where $\beta \sim 0.2-0.3$ and is therefore associated with the switching of the channel modes rather than with a small change in the local potential.

The important prediction of a suppression of the shot noise in ballistic QPCs (see Section 4.1.5 above) has motivated many recent experiments of the noise properties of QPCs. Broadband measurements performed at high frequencies (8 – 18 GHz) [95R, 96R] have shown an interesting suppression of the shot noise which scales linearly with the applied source-drain bias and whose maxima are approximately given by $(1/4)2e(2e^2/h)V_{\mathrm{sd}}$, in agreement with the theories discussed above. Typical measurements are shown in Fig. 103; the observed shift of the noise maxima relative to the points of inflection between plateaux is not yet understood. Nevertheless, the correlated transport of electrons in ballistic QPCs is confirmed, and it is speculated that this arises from the

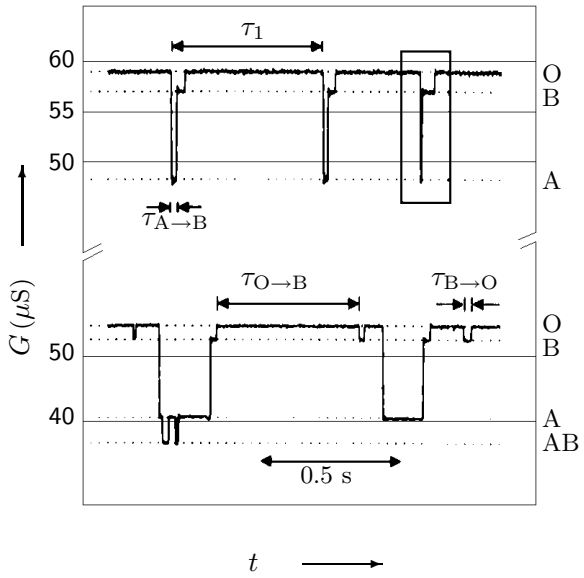

Fig. 102: The conductance of a ballistic QPC at two fixed gate voltages between pinch-off and the first quantized plateau as measured in the time domain [91C]. The inset box shows the suprising irreversible switching behaviour.

Coulomb interaction between carriers.

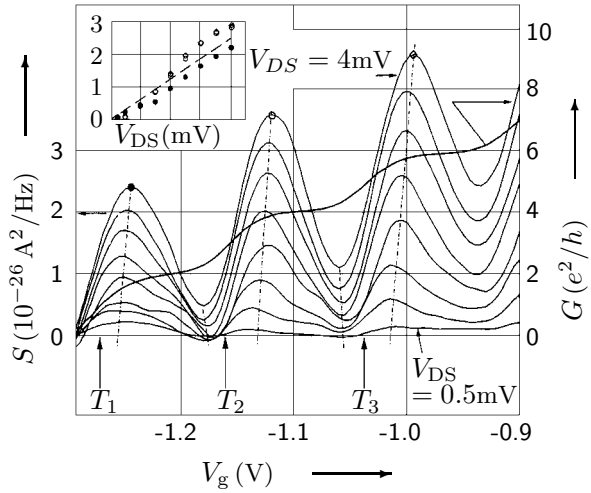

Fig. 103: The noise spectral density and the conductance (for a bias current of 10 nA) are plotted as a function of the applied gate voltage. The arrows indicate the positions ($T_n = 1/2$, $n = 1, 2, 3$) where maxima of the noise are expected. The inset shows the observed dependence of the noise maxima upon the applied source-drain bias; the theoretical prediction is also indicated [96R].

The most convincing experimental verification of the shot noise theory has been found in the low-temperature measurments performed at low-frequencies (1 – 10 kHz) [96K4]. The shot noise observed has a frequency independent spectrum over at least one decade and shows the linear variation with bias current for $V_{sd} > 4k_BT/e$. The expected reduction of the noise spectrum, which scales with $(1 - T_1)$ for the lowest subband, is clearly demonstrated, as shown in Fig. 104. The saturation at low bias is simply the recovery of the expected equilibrium noise result. Other recent experiments [96K5, 97K2] designed to test the influence of the Pauli exclusion principle on the noise statistics of QPCs have been hampered by the large noise levels associated with the switching phenomena discussed above.

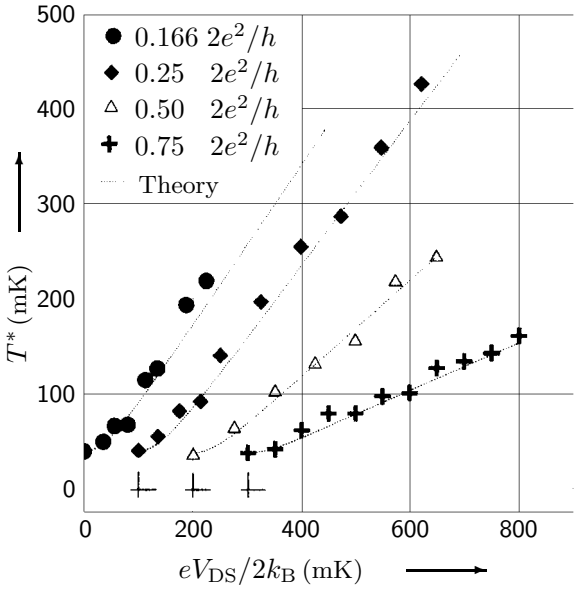

Fig. 104: The noise temperature is plotted as a function of the applied bias (in appropriate temperature units) for different values of the transmission at fixed temperature, $T = 384\,\mathrm{mK}$. The curves are offset by 100 mK for clarity [96K4].

4.7 References for Section 4

[56HB] Hanbury Brown, R., Twiss, R.Q.: Nature **177** (1956) 27.

[63T] Tien, P.K., Gordon, J.P.: Phys. Rev. **129** (1963) 647.

[89C] Cahay, M., Kreskovsky, J.P., Grubin, H.L.: Solid-State Electronics **32** (1989) 1185.

[89L2] Lesovik, G.B.: JETP Lett. **49** (1989) 515.

[90B3] Büttiker, M.: Phys. Rev. Lett. **65** (1990) 2901.

[90L] Li, Y.P., Tsui, D.C., Heremans, J.J., Simmons, J.A., Weimann, G.W.: Appl. Phys. Lett. **57** (1990) 774.

[90T2] Timp, G., Behringer, R.E., Cunningham, J.E.: Phys. Rev. B **42** (1990) 9259.

[90Y2] Yurke, B., Kochanski, G.P.: Phys. Rev. B **41** (1990) 8184.

[91C] Cobden, D.H., Patel, N.K., Pepper, M., Ritchie, D.A., Frost, J.E.F., Jones, G.A.C.: Phys. Rev. B **44** (1991) 1938.

[91D] Dekker, C., Scholten, A.J., Liefrink, F., Eppenga, R., van Houten, H., Foxon, C.T.: Phys. Rev. Lett. **66** (1991) 2148.

[91H1] Hekking, F.W.J., Nazarov, Yu.V.: Phys. Rev. B **44** (1991) 11506.

[91H2] Hekking, F.W.J., Nazarov, Yu.V., Schön, G.: Europhys. Lett. **14** (1991) 489.

[91L2] Liefrink, F., Scholten, A.J., Dekker, C., Eppenga, R., van Houten, H., Foxon, C.T.: Physica B **175** (1991) 213.

[92B2] Büttiker, M.: Phys. Rev. B **46** (1992) 12485.

[92C2] Cobden, D.H., Savchenko, A., Pepper, M., Patel, N.K., Ritchie, D.A., Frost, J.E.F., Jones, G.A.C.: Phys. Rev. Lett. **69** (1992) 502.

[92E] Endoh, A., Sasa, S., Muto, S.: Appl. Phys. Lett. **61** (1992) 52.

[92EY] Eric Yang, S.-R.: Solid State Communications **81** (1992) 375.

[92L1] Levinson, I.B., Shapiro, B.: Phys. Rev. B **46** (1992) 15520.

[92L2] Liefrink, F., Scholten, A.J., Dekker, C., Dijkhuis, J.I., Alphenaar, B.W., van Houten, H., Foxon, C.T.: Phys. Rev. B **46** (1992) 15523.

[92T4] Taylor, R.P., Fortin, S., Sachrajda, A.S., Adams, J.A., Fallahi, M., Davies, M., Coleridge, P.T., Zawadzki, P.: Phys. Rev. B **45** (1992) 9149.

[93F1] Fedichkin, L., Ryzhii, V.I., V'yurkov, V.V.: J. Phys.: Condens. Matter **5** (1993) 6091.

[93F2] Feng, S., Hu, Q.: Phys. Rev. B **48** (1993) 5354.

[93H2] Hu, Q.: Appl. Phys. Lett. **62** (1993) 837.

[93W] Wyss, R.A., Eugster, C.C., del Alamo, J.A., Hu, Q.: Appl. Phys. Lett. **63** (1993) 1522.

[94G1] Gödel, W., Manus, S., Wharam, D.A., Kotthaus, J.P., Böhm, G., Klein, W., Tränkle, G., Weimann, G.: Electron. Lett. **30** (1994) 977.

[94G2] Grincwajg, A., Jonson, M., Shekhter, R.I.: Phys. Rev. B **49** (1994) 7557.

[94J] Janssen, T.J.B.M., Maan, J.C., Singleton, J., Patel, N.K., Pepper, M., Frost, J.E.F., Ritchie, D.A., Jones, G.A.C.: J. Phys.: Condens. Matter **6** (1994) L163.

[94K2] Karadi, C., Jauhar, S., Kouwenhoven, L.P., Wald, K.R., Orenstein, J., McEuen, P.L., Nagamune, Y., Sakaki, H.: J. Opt. Soc. Am. B. **11** (1994) 2566.

[94L2] Liefrink, F., Dijkhuis, J.I., van Houten, H.: Semicond. Sci. Technol. **9** (1994) 2178.

[94Z] Zagoskin, A.M., Shekhter, R.I.: Phys. Rev. B **50** (1994) 4909.

[95A] Arnone, D.D., Frost, J.E.F., Smith, C.G., Ritchie, D.A., Jones, G.A.C., Butcher, R.J., Pepper, M.: Appl. Phys. Lett. **66** (1995) 3149.

[95G] Grincwajg, A., Gorelik, L.Y., Kleiner, V.Z., Shekhter, R.I.: Phys. Rev. B **52** (1995) 12168.

[95H1] Hessling, J.P., Galperin, Yu.M.: Phys. Rev. B **52** (1995) 5082.

[95H2] Hessling, J.P., Galperin, Yu.M., Jonson, M., Shekhter, R.I., Zagoskin, A.M.: J. Phys.: Condens. Matter **7** (1995) 7239.

[95R] Reznikov, M., Heiblum, M., Shtrikman, H., Mahalu, D.: Phys. Rev. Lett. **75** (1995) 3340.

[95S1] Sakamoto, T., Nakamura, Y., Hwang, S., Nakamura, K.: Jpn. J. Appl. Phys. **34** (1995) 4302.

[95W] Wyss, R.A., Eugster, C.C., del Alamo, J.A., Hu, Q., Rooks, M.J., Melloch, M.R.: Appl. Phys. Lett. **66** (1995) 1144.

[96H] Hu, Q., Verghese, S., Wyss, R.A., Schäpers, T., del Alamo, J.A., Feng, S., Yakubo, K., Rooks, M.J., Melloch, M.R., Förster, A.: Semicond. Sci. Technol. **11** (1996) 1888.

[96K4] Kumar, A., Saminadayar, L., Glattli, D.C., Jin, Y., Etienne, B.: Phys. Rev. Lett. **76** (1996) 2778.

[96K5] Kurdak, Ç., Chen, C.-J., Tsui, D.C., Lu, J.P., Shayegan, M., Parihar, S., Lyon, S.A.: Surf. Sci. **361/362** (1996) 705.

[96M1] Maaø, F.A.: J. Phys.: Condens. Matter **8** (1996) L625.

[96M2] Maaø, F.A., Gorelik, L.Y.: Phys. Rev. B **53** (1996) 15885.

[96R] Reznikov, M., Heiblum, M., Shtrikman, H., Mahalu, D.: Surf. Sci. **361/362** (1996) 726.

[96S1] Shilton, J.M., Mace, D.R., Talyanskii, V.I., Galperin, Yu.M., Simmons, M.Y., Pepper, M., Ritchie, D.A.: J. Phys.: Condens. Matter **L337** (1996) 8.

[96S2] Shilton, J.M., Talyanskii, V.I., Pepper, M., Ritchie, D.A., Frost, J.E.F., Ford, C.J.B., Smith, C.G., Jones, G.A.C.: J. Phys.: Condens. Matter **L531** (1996) 8.

[96S3] Smith, J.C., Berven, C., Wybourne, M.N., Goodnick, S.M.: Surf. Sci. **361/362** (1996) 656.

[97H2] Haubrich, A.G.C., Wharam, D.A., Kriegelstein, H., Manus, S., Lorke, A., Kotthaus, J.P., Gossard, A.C.: Appl. Phys. Lett. **70** (1997) 3251.

[97K2] Kurdak, Ç., Chen, C.-J., Tsui, D.C., Parihar, S., Lyon, S.A., Weimann, G.W.: Phys. Rev. B **56** (1997) 9813.

[97S1] Schoelkopf, R.J., Burke, P.J., Kozhevnikov, A.A, Prober, D.E., Rooks, M.J.: Phys. Rev. Lett. **78** (1997) 3370.

[97S2] Smith, J.C., Wybourne, M.N., Berven, C., Ramasubramaniam, R., Goodnick, S.M.: Europhys. Lett. **39** (1997) 73.

[97T1] Tageman, O., Gorelik, L.Y., Shekhter, R.I., Jonson, M.: J. Appl. Phys. **81** (1997) 285.

[97T2] Totland, H., Bø, Ø.L., Galperin, Yu.M.: Phys. Rev. B **56** (1997) 15299.

[97W] Wagner, M., Zwerger, W.: Phys. Rev. B **55** (1997) 10217.

[98P] Pedersen, M.H., van Langen, S.A., Büttiker, M.: Phys. Rev. B **57** (1998) 1838.

[98T] Tageman, O., Gorelik, L.Y.: J. Appl. Phys. **83** (1998) 1513.

[99C] Cuniberti, G., Fechner, A., Sassetti, M., Kramer, B.: Europhys. Lett. **48** (1999) 66.